

# Comparison of microporous/mesoporous and microporous HZSM-5 as catalysts for Friedel–Crafts alkylation of toluene with ethene

Cite this: *RSC Adv.*, 2014, 4, 28786Zebastian Bohström,<sup>\*a</sup> Hanna Härelind,<sup>b</sup> Börje Gevert,<sup>a</sup> Sven-Ingvar Andersson<sup>a</sup> and Krister Holmberg<sup>\*a</sup>

In this work we investigated the effect of mesopores in a standard zeolite used as a catalyst for Friedel–Crafts alkylation of toluene with ethene. A cationic polymer was used for templating mesopores in a microporous ZSM-5 framework. The mesopore-containing zeolite was compared with a regular zeolite with only micropores with respect to conversion, yield and selectivity. The two NaZSM-5 materials were prepared with the same Si/Al molar ratio and diffuse reflection infrared Fourier transform spectroscopy (DRIFT-FTIR) confirmed that the acidity of the ion-exchanged forms (HZSM-5) were identical. Scanning electron microscopy (SEM) and dynamic light scattering (DLS) were used to determine the particle size of the zeolites, which was similar for the two HZSM-5 materials and nitrogen sorption was used to determine the surface area and pore size distribution. X-ray diffraction (XRD) analysis displayed typical crystalline diffraction patterns for the ZSM-5 framework for both the microporous/mesoporous and the microporous ZSM-5 materials. The results from catalytic testing show an increase in the overall conversion of toluene for the zeolite that contains mesopores. Furthermore, a higher product yield ( $C_9$ ) is obtained for this catalyst. The increase in yield and conversion is most likely due to the mesopores; however, incorporation of mesopores in the microporous ZSM-5 framework gives only minor effects on selectivity with respect to mono- vs. dialkylation, and *ortho* : *meta* : *para* ratio. Consequently, this work shows that the presence of mesopores in a microporous ZSM-5 framework is beneficial for the reaction in terms of conversion of starting material and reaction yield but does not markedly affect the product composition.

Received 9th March 2014

Accepted 10th June 2014

DOI: 10.1039/c4ra02056a

[www.rsc.org/advances](http://www.rsc.org/advances)

## Introduction

Microporous zeolites are extensively used as catalysts in industry.<sup>1</sup> However, microporous catalysts are often associated with efficiency problems such as short lifetime and poor mass transport.<sup>2</sup> The small pores are easily clogged by carbonaceous material, in particular when the reaction temperature is high. Mesoporous catalysts do not exhibit the same mass transport and lifetime limitations as microporous catalysts.<sup>3</sup> On the other hand, the use of mesoporous catalysts in industrial processes is often restricted by the low hydrothermal stability of the material.<sup>4</sup> Furthermore, large pore catalysts sometimes lack the isomer selectivity that can sometimes be obtained with microporous catalysts.<sup>5</sup>

Thus, both microporous and mesoporous catalysts have specific desirable properties, as well as specific drawbacks associated with the character of the pores. It would therefore be advantageous to combine, in one material, the favorable properties of microporous catalysts with those of mesoporous catalysts, thereby obtaining a uniquely versatile catalyst. Efforts have recently been made to prepare mesoporous zeolites.<sup>6</sup> It has been shown that depending on the preparation route and the synthesis conditions zeolites with different populations of micro- and mesopores can be obtained. In this work we prepared microporous zeolites with mesopores penetrating the structure. The crystalline micropore structure is of MFI-type (ZSM-5). The performance of this microporous/mesoporous ZSM-5 zeolite has been studied in the Friedel–Crafts alkylation of toluene with ethene. In addition, we prepared a conventional microporous ZSM-5 zeolite and compared its catalytic activity with that of the microporous/mesoporous ZSM-5. The two ZSM-5 zeolites were prepared with the same Si/Al weight ratio in order to ensure that differences in acidity and activity of the catalysts are due to differences in structure, not in composition. The optimum conversion of toluene into ethyltoluene over

<sup>a</sup>Department of Chemical and Biological Engineering, Applied Surface Chemistry, Chalmers University of Technology, SE-412 96 Göteborg, Sweden. E-mail: [kh@chalmers.se](mailto:kh@chalmers.se); [zebastian.bohstrom@chalmers.se](mailto:zebastian.bohstrom@chalmers.se); Fax: +46 31 16 00 62; Tel: +46 31 772 29 69

<sup>b</sup>Department of Chemical and Biological Engineering and Competence Centre for Catalysis, Chalmers University of Technology, SE-412 96 Göteborg, Sweden

zeolitic catalysts is reported to lie in the temperature range from 300 °C to 350 °C.<sup>7</sup>

## Experimental

### Materials and reagents

Sodium aluminate (Sigma-Aldrich, technical), tetrapropylammonium hydroxide solution (Sigma-Aldrich, 1 M in H<sub>2</sub>O), tetraethyl orthosilicate (Sigma-Aldrich) and poly(diallyldimethylammonium chloride) (Aldrich, 65 wt% in H<sub>2</sub>O) were used to prepare the NaZSM-5 zeolites. Ammonium nitrate (A.C.S. reagent ≥ 98%), LiBO<sub>2</sub>·H<sub>2</sub>O (Aldrich) and nitric acid (Sigma-Aldrich, A.C.S. 70%) were used to ion-exchange the zeolites from Na-form to H-form. Toluene (Sigma-Aldrich, 99.9%) and ethene gas (AGA, 95%, containing 3 ± 2 mol% nitrogen) were used for the alkylation reaction. 2-Ethyltoluene (purum, ≥98%, FLUKA), 3-ethyltoluene (purum, ≥98%, FLUKA) and 4-ethyltoluene (≥95%, FLUKA) were used for identification of relative amounts of ethyltoluene isomers in the liquid samples produced from the continuous reactor.

### Preparation of ZSM-5 zeolites

The microporous and microporous/mesoporous ZSM-5 zeolites were prepared by essentially following the procedure described by Wang *et al.*<sup>8</sup> Sodium aluminate (1.12 g), tetraethyl orthosilicate (39.76 g) and tetrapropylammonium hydroxide (56.0 g) were added to distilled water (140.0 g) and aged at 100 °C under stirring for 3 h. Then the polymer poly(diallyldimethylammonium chloride) (10 wt%, 42.0 g) was added to the mixture. For the preparation of the microporous ZSM-5 no polymer was added. After stirring at room temperature for 48 h, the reaction mixture was transferred into an autoclave and crystallised at 180 °C for 144 h. The product was collected by centrifugation and calcined at 550 °C for 5 h with 1 h ramping.

### Preparation of the zeolites in H-form

The Na-zeolites were converted into H-zeolite following the procedure described by Punyapalakul *et al.*<sup>9</sup> Ammonium nitrate solution (1.0 M) was mixed with the zeolite at a ratio of 1 : 20, solid : liquid. The mixture was stirred at 60 °C for 2 h, filtered and washed with Milli-Q water (18.2 MΩ cm). This exchange procedure was repeated. The solid was collected and dried at 100 °C for 12 h and then calcined at 400 °C for 3 h with a 6 h ramping. The degree of ion-exchange was determined with atomic absorption spectroscopy. The first ion-exchange cycle resulted in a 42% exchange of the sodium content in the sample. After two cycles 87% of the sodium had been exchanged.

### Friedel–Crafts alkylation reactor setup

The Friedel–Crafts alkylation reactions were performed in a fixed bed down-flow reactor with an internal diameter of 10 mm and a length of 175 mm. The reactor was equipped with a heating jacket and a high sensitivity temperature controller. The setup was designed to carry out a vapour phase reaction

under atmospheric pressure. Before the experiments the fixed bed reactor was packed with quartz wool, followed by a layer of glass pellets and another layer of quartz wool. Next, the catalyst powder was added to the reactor and packed tightly. The catalyst powder (4.0 g) consisted of a mixture of zeolite powder (1.25 g) and silicon powder (2.75 g). Subsequently, quartz wool was added on top of the catalyst powder and finally a layer of glass pellets was applied (Table 1).

The reactor was heated to the reaction temperature and ethene was introduced into the system over heated liquid toluene. The ethene–toluene gas mixture (1 : 1) was fed into the reactor and then separated in a cooling trap with cold glycerol (for flow rates, see Table 2). The gas leaving the cooling trap was periodically analysed and directly fed into a Perkin Elmer Clarus 500 GC equipped with a flame ionization detector (FID-GC) and a thermal conductivity detector (TCD). The condensed products collected in the cooling trap were analysed qualitatively with a GC-MS setup and quantitatively with a GC-FID setup.

### Analysis techniques

Determination of the specific surface area was performed on an ASAP 2010 instrument, using nitrogen adsorption and calculated with the BET (Brunauer–Emmett–Teller) method.<sup>10</sup> The pore size distribution was calculated from the isotherms using the BJH (Barett–Joyner–Halenda) procedure.<sup>11</sup> All samples were dried at 225 °C in a vacuum oven for approximately 3 h before the measurement.

Samples for scanning electron microscopy (SEM) were run on a LEO, Ultra, 55 FEG, SEM equipped with an Oxford Inca EDX system operated at 1–2 kV. A secondary electron detector was used for detection. Samples for SEM were prepared by dispersing a small amount of zeolite in ethanol and then grinding the mixture and placing a droplet onto the metallic sample holder.

Samples for transmission electron microscopy (TEM), run on a JEOL 1200 EX II instrument at 120 kV, were prepared by placing a drop of an ethanol dispersion of the zeolitic material onto a copper Holey grid.

*In situ* FTIR (Fourier Transform Infrared) spectroscopy measurements were carried out using a BioRad FTS 6000 spectrometer equipped with a Harrick Praying Mantis DRIFT (Diffuse Reflection Infrared Fourier Transform) reaction cell.<sup>12</sup> The sample was put in the DRIFT cell and the gases; Ar, NH<sub>3</sub> and O<sub>2</sub> were introduced *via* mass flow controllers (Bronkhorst Hi-Tech) to the cell. The samples were initially pre-treated in O<sub>2</sub> (8%) at 500 °C for 30 minutes and then evacuated in Ar for 15 minutes (keeping the total flow rate constant at 200 ml min<sup>-1</sup>). Adsorption of NH<sub>3</sub> (1000 ppm) was performed at 25 °C during 30 minutes, followed by evacuation in Ar (6 scans per min, 1 cm<sup>-1</sup> resolution). Background spectra were collected in Ar (6 scans per min, 1 cm<sup>-1</sup> resolution).

X-ray powder diffraction (XRD) was performed on a LynxEye AXS D8 ADVANCE  $\theta/2\theta$  diffractometer, equipped with a linear detector. The runs were performed at 40 kV and 40 mA, in monochromatic mode with G(111) CuK $\alpha$ 1 radiation

( $\lambda = 1.5406 \text{ \AA}$ , step size 0.050, step time 366 s and primary slit width 0.2 mm).

Atomic absorption spectroscopy was performed on a Thermo Scientific ICE 3000 Series AA spectrometer. The solid catalyst (100 mg) was mixed with  $\text{LiBO}_2 \cdot \text{H}_2\text{O}$  (1.0 g) in a platinum crucible and the mixture was heated at  $1000 \text{ }^\circ\text{C}$  for 13 minutes. When the crucible had cooled to room temperature, aqueous nitric acid (3 wt%) was added (1.5–3.0 ml) and the mixture in the platinum crucible was stirred at 300 rpm for 6 h. The content in the crucible was added to a 25 ml flask and aqueous nitric acid (3 wt%) was added to the 25 ml mark. A flame was used to atomize the sample and a sodium hollow cathode lamp was used for the irradiation.

Dynamic light scattering (DLS) was performed on a BI-90 Brookhaven Instruments particle sizer. Samples were prepared by taking a small fraction of the solid material and dispersing it into a glass beaker containing 5.0 ml filtered (0.2  $\mu\text{m}$  filter) Milli-Q water (18.2  $\text{M}\Omega \text{ cm}$ ). The beaker was immersed in a sonic bath for 1 minute. 3.0 ml of this solution was then transferred into another glass beaker containing 3.0 ml filtered (0.2  $\mu\text{m}$  filter) Milli-Q water. This beaker was then immersed into a sonic bath for 1 minute and 2.5 ml of this solution was transferred into the quartz cuvette with a syringe fitted with a 1.2  $\mu\text{m}$  filter and analysed.

Flame ionization and thermal conductivity gas chromatography (FID-GC and TCD-GC, respectively) was performed on a PE Clarus 500 GC and used to monitor the gaseous products formed during the reaction. The instrument was fitted with a standard RGA Model 1115 Analyser GC column set. The injector temperature was  $50 \text{ }^\circ\text{C}$ , helium was used as carrier gas and nitrogen was the actuator gas. Both gases were kept at a pressure of 6.2 bars. The gases were used at a flow rate of  $0.91 \text{ ml min}^{-1}$  and the splitflow was  $50 \text{ ml min}^{-1}$ . The TCD detection temperature was  $200 \text{ }^\circ\text{C}$  and the current used for the detector was 40 mA. The FID detection temperature was  $250 \text{ }^\circ\text{C}$ . Samples from the continuous reactor (5.0  $\mu\text{l}$ ) were introduced from a 0.125 and a 1.0  $\text{cm}^3$  gas loop valve into the GC. The analysis was performed during 15 minutes at a temperature of  $60 \text{ }^\circ\text{C}$ . The liquid product formed during the reaction was analysed qualitatively with GC-MS and quantitatively with a GC-FID setup. The GC-MS analysis was performed with a HP5890 gas chromatograph coupled to a thermo trace mass spectrometer and the GC was fitted with an Agilent J&W DB-5MS,  $30 \text{ m} \times 0.25 \text{ mm} \times 1.0 \mu\text{m}$  column. The analysis was performed with an injector temperature of  $200 \text{ }^\circ\text{C}$ , helium was used as the carrier gas at a flow of  $1.2 \text{ ml min}^{-1}$ , the splitflow was  $40 \text{ ml min}^{-1}$  and the scans performed at a mode of 40–300 amu at an ion source temperature of  $200 \text{ }^\circ\text{C}$ . The temperature program used started at  $40 \text{ }^\circ\text{C}$  and was maintained at that temperature for 3 min, then ramped to  $125 \text{ }^\circ\text{C}$  at a rate of  $4 \text{ }^\circ\text{C min}^{-1}$ , then increased from  $125 \text{ }^\circ\text{C}$  to  $150 \text{ }^\circ\text{C}$  at a rate of  $2.5 \text{ }^\circ\text{C min}^{-1}$ , and finally went from  $150 \text{ }^\circ\text{C}$  to  $200 \text{ }^\circ\text{C}$  at a rate of  $5.0 \text{ }^\circ\text{C min}^{-1}$ . For the quantitative GC-FID analysis the same GC column and temperature program was used for the qualitative GC-MS analysis. The injector temperature was  $275 \text{ }^\circ\text{C}$ , helium was used as carrier gas at a flow of  $0.92 \text{ ml min}^{-1}$  and the splitflow was  $40 \text{ ml min}^{-1}$ . The FID detection temperature was

$275 \text{ }^\circ\text{C}$ . Toluene, *para*-ethyltoluene, *meta*-ethyltoluene and *ortho*-ethyltoluene were injected into the GC-MS setup to identify the specific retention times of each of these compounds.

## Results and discussion

### The microporous and the microporous/mesoporous ZSM-5 zeolites

Two different types of zeolites were prepared, microporous NaZSM-5 and microporous/mesoporous NaZSM-5. The zeolites were prepared with the same Si/Al molar ratio. In Fig. 1 the diffractograms of the two NaZSM-5 zeolites are shown. The crystalline structure displayed is typical for the ZSM-5 zeolite type.<sup>13</sup> In addition, no difference in intensities was observed between the two ZSM-5 zeolites. The microporous NaZSM-5 displayed a nitrogen sorption isotherm of *Type I* with a *H4* hysteresis characteristic for microporous materials,<sup>14</sup> see Fig. 2. The microporous/mesoporous NaZSM-5 displayed a *Type IV* sorption isotherm and a *H3* hysteresis. The *Type IV* sorption isotherm is typical for mesoporous materials.<sup>14</sup> *H3* hysteresis has been interpreted as an intermediate between *H1* and *H4* hysteresis curves.<sup>14</sup> The hysteresis ranging from 0.8 to 0.95 seen for the microporous/mesoporous NaZSM-5 zeolite is indicative of hierarchical mesopores.<sup>8</sup> *In situ* DRIFT experiments with ammonia adsorption followed by argon flushing were performed in order to characterize the surface acidity of the samples and the results are shown in Fig. 3. When ammonia is adsorbed on the microporous HZSM-5 sample multiple peaks at 3395, 3275 and  $1288 \text{ cm}^{-1}$  evolve. These peaks can, according to Wang *et al.* and Tsyganenko *et al.*, be ascribed to  $\text{NH}_3$  adsorbed on Lewis acid sites.<sup>15</sup> Another group of peaks at 1572 and  $1510 \text{ cm}^{-1}$  can be attributed to  $\text{NH}_2$  surface species formed concurrently with OH groups during ammonia dissociation.<sup>15</sup> Furthermore, the negative peaks at 3689 and  $3610 \text{ cm}^{-1}$  are indicative of blocking of surface OH species by adsorbed  $\text{NH}_3$ .<sup>15</sup> Similar peaks evolve upon addition of ammonia to the microporous/mesoporous HZSM-5. No significant differences are observed for the two samples, indicating that the acidic sites are similar. This is not surprising since the composition of the two

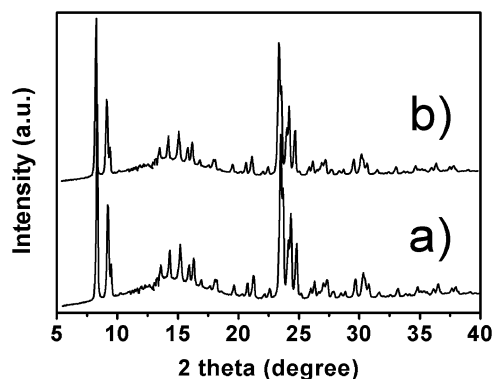


Fig. 1 XRD diffractograms of the (a) microporous and (b) the microporous/mesoporous NaZSM-5.

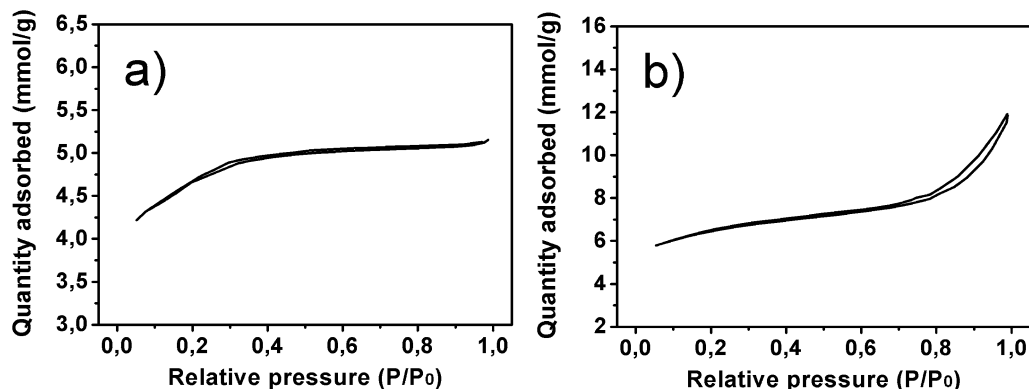


Fig. 2 Nitrogen sorption isotherms of microporous NaZSM-5 and microporous/mesoporous NaZSM-5.

zeolites is the same. Fig. 4 shows scanning electron microscopy (SEM) images of the microporous and the microporous/mesoporous NaZSM-5 zeolites, as well as transmission electron microscopy (TEM) micrograph of the microporous/mesoporous NaZSM-5. The SEM images show that the particle size is similar for the two zeolites. The morphology of the particles is very different, however. Whereas the microporous zeolite particles have a smooth surface and round edges, the microporous/mesoporous zeolite particles are very rough. They appear to consist of granules glued together. The TEM image analysis indicates that the granules are porous or hollow. From the data

presented above one can conclude that the microporous and the microporous/mesoporous ZSM-5 zeolites are very similar in terms of particle size, specific surface area and chemical composition, including acidic surface sites. However, as indicated by both the nitrogen sorption analysis and the electron microscopy images the ZSM-5 prepared with a polymer template contains pores not only in the micro size but also in the meso size range. Thus, any difference in yield, rate or selectivity of an organic reaction where these materials are used as catalyst can be attributed to the presence of mesopores in one of the zeolites.

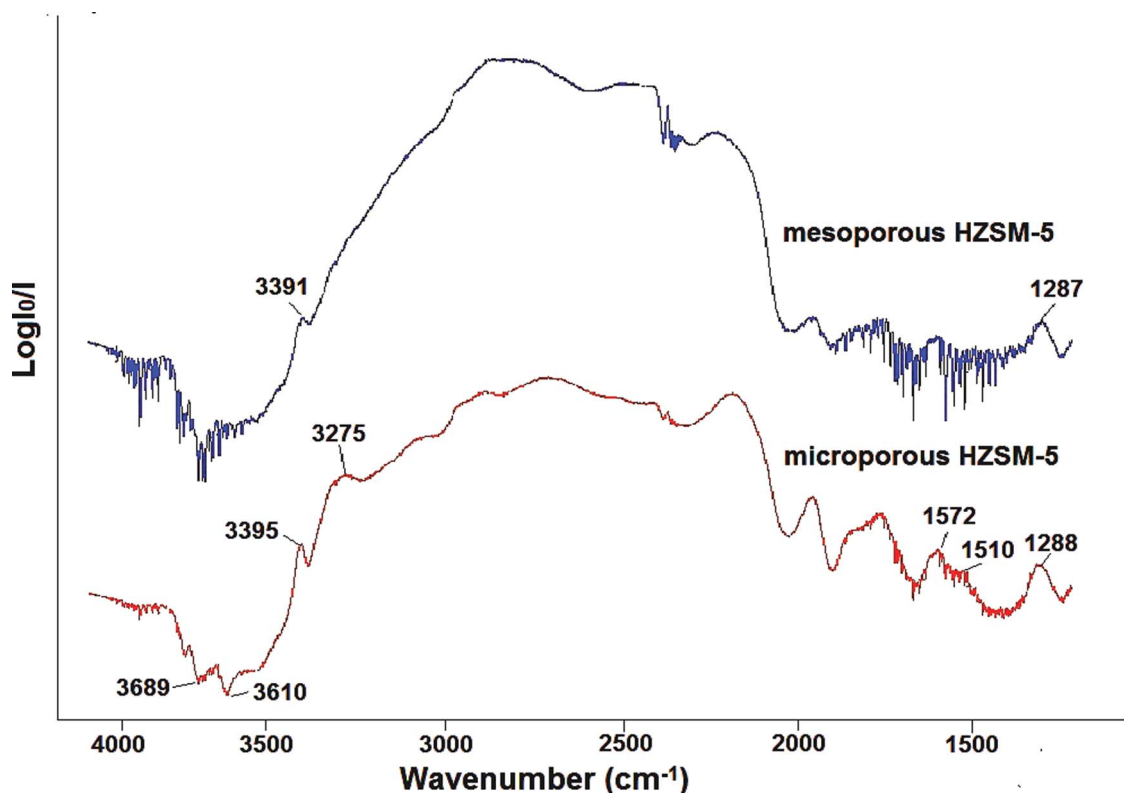


Fig. 3 DRIFT spectra showing surface  $\text{NH}_3$  and  $\text{NH}_4^+$  species after adsorption of ammonia during 30 minutes followed by argon flushing during 30 minutes.

**Table 1** Zeolite characteristics obtained from nitrogen sorption data, dynamic light scattering (DLS) and scanning electron microscopy (SEM)

Zeolite	Nitrogen sorption						Average particle size (nm)	
	$a_{s,BET}^a$ ( $m^2 g^{-1}$ )	Calculated <sup>b</sup> ( $r$ , nm)	Measured <sup>c</sup> ( $r$ , nm)	$P_{vol}^c$ ( $cm^3 g^{-1}$ )	Micro $_{vol}^d$ ( $cm^3 g^{-1}$ )	$V_{tot}^a$ ( $cm^3 g^{-1}$ )	DLS <sup>e</sup>	SEM <sup>f</sup>
Micro/mesoporous ZSM5	380	1.32	3.61	0.10	0.13	0.25	312 ± 26	350 ± 80
Microporous ZSM5	372	0.91	—	—	0.11	0.17	328 ± 38	340 ± 110

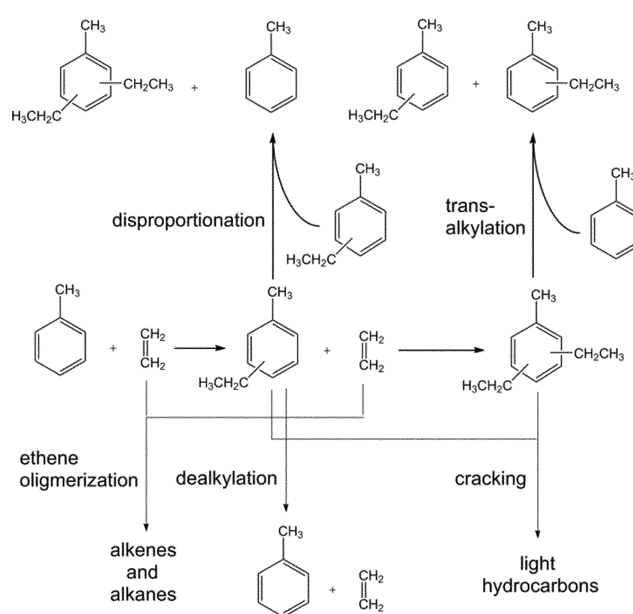
<sup>a</sup> Calculated from nitrogen sorption using the BET method. <sup>b</sup> Calculated  $2V_{tot}/S_{BET}$ . <sup>c</sup> Calculated from the adsorption branch of the nitrogen sorption isotherm using the BJH method. <sup>d</sup> Calculated from  $t$ -plot. <sup>e</sup> Particle size determined from DLS analysis presented as means of 4 independent runs. <sup>f</sup> Particle size determined with SEM. The values reported are means of 50 particles.

### The Friedel–Crafts alkylation reaction

Alkylation of toluene over zeolitic catalysts has been the topic of many studies. The activity and selectivity of conventional microporous zeolites, in particular HZSM-5 zeolites, have been investigated indepth.<sup>16</sup> In this study we have investigated and compared the conversion, yield and regioselectivity of the microporous and the microporous/mesoporous HZSM-5 zeolites as catalysts for the Friedel–Crafts alkylation of toluene with ethene. However, before any catalytic testing were performed the mesoporous/microporous and microporous ZSM-5 zeolites thermal and hydrothermal stability was investigated. It was found that the mesoporous/microporous ZSM-5 was stable under temperatures and conditions used for catalytic testing.

Alkylations at high temperatures in continuous flow-bed reactors usually give rise to several side reactions that occur in parallel to the target alkylation reaction. Transalkylation, disproportionation, dealkylation and catalytic cracking are examples of such side reactions<sup>17</sup> and they are illustrated in Scheme 1 for the toluene–ethene system. Furthermore, previous studies at our laboratory have shown that ethene starts to undergo zeolite-catalyzed oligomerization at temperatures around 320 °C. Catalytic cracking over HZSM-5 zeolites is generally performed at temperatures ranging from 550 °C to 650 °C.<sup>18</sup> However, catalytic cracking occurs also at lower temperatures.<sup>19</sup> Suza *et al.* recently reported that at 350 °C there was 10–13% cracking conversion of natural gasoline in a continuous flow reactor.<sup>19b</sup> All these side reactions give rise to other products than the target product of the Friedel–Crafts reaction, *i.e.*, ethyltoluene (and possibly some diethyltoluene) and these products will all appear in the liquid fraction from the reaction. GC analysis showed that the yield of C<sub>5</sub>–C<sub>11</sub> products

in the gaseous fraction from the reaction was negligible. Whereas the conversion of ethene is quantitative already at 325 °C with the microporous/mesoporous catalyst, reaction over the conventional microporous zeolite did not reach full ethene conversion until the temperature reached 375 °C. This indicates a slightly higher activity of the catalyst that contains mesopores. The figures for toluene conversion give the same picture; the catalyst with mesopores seems to be more active. The



**Scheme 1** Friedel–Crafts alkylation of toluene with ethene and possible side reactions.

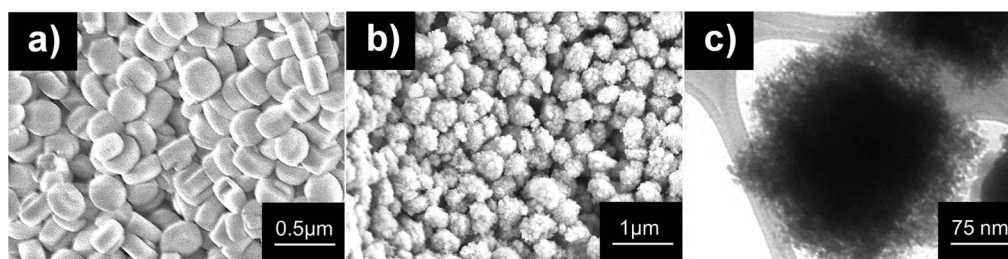


**Fig. 4** (a and b) are SEM images of the microporous and the microporous/mesoporous NaZSM-5, respectively. (c) is a TEM image of the microporous/mesoporous NaZSM-5.

Table 2 Yield of C<sub>5</sub>–C<sub>11</sub> hydrocarbons obtained with the microporous/mesoporous HZSM-5 and microporous HZSM-5 at various conditions

Catalyst	Microporous/mesoporous HZSM-5						Microporous HZSM-5			
	325	350	375	400	375	375	325	350	375	400
Temperature (°C)	325	350	375	400	375	375	325	350	375	400
Flow (ml min <sup>-1</sup> )	30	30	30	30	15	60	30	30	30	30
Toluene conversion <sup>a</sup> (%)	32	61	70	65	70	68	46	49	49	41
Ethene conversion <sup>b</sup> (%)	>99	>99	>99	>99	>99	97	93	95	>99	>99
<b>Products (wt%)</b>										
C <sub>5</sub>	n.d.	5.9	5.7	5.2	4.4	3.9	4.0	1.2	0.4	0.2
C <sub>6</sub>	n.d.	0.4	0.4	0.1	0.3	0.2	0.3	0.3	0.1	n.d.
C <sub>7</sub>	73	38	30	32	28	30	54	56	57	66
C <sub>8</sub>	n.d.	3.5	3.8	12	5.7	10	0.5	0.2	n.d.	n.d.
C <sub>9</sub>	25	40	46	37	44	38	27	34	34	30
C <sub>10</sub>	1	5.6	8.0	5.7	9.8	7.7	6.7	2.4	2.0	0.1
C <sub>11</sub>	1	5.1	6.0	5.9	6.2	6.7	6.5	5.9	6.5	3.7
C <sub>12</sub>	n.d.	0.5	0.1	2.0	1.6	3.4	n.d.	n.d.	n.d.	n.d.
C <sub>13</sub>	n.d.	n.d.	n.d.	0.1	n.d.	0.1	n.d.	n.d.	n.d.	n.d.
Ethyltoluene C <sub>9</sub>	24	38	45	34	42	37	23	33	34	29
<i>Ortho</i>	—	3	6	9	9	8	1	6	6	7
<i>Meta</i>	48	55	58	59	61	62	54	56	57	56
<i>Para</i>	52	42	36	32	30	30	45	38	37	37
Mono/di ratio <sup>c</sup>	20.3	6.4	6.2	4.8	5.8	4.6	3.4	4.7	4.2	6.6

<sup>a</sup> Calculated from C<sub>7</sub>, C<sub>9</sub> and C<sub>11</sub> molar fraction in the liquid samples. <sup>b</sup> Calculated from *in situ* GC with TCD detector. <sup>c</sup> Mol ratio. n.d. = not detected.

conversion of toluene is clearly temperature dependent, in particular for the microporous/mesoporous catalyst, but it never reaches above 70%. The obvious interpretation of these results is that ethene is a very reactive reactant, which participates in reactions other than the Friedel–Crafts alkylation, see the discussion above. When it comes to product distribution, the C<sub>7</sub> and the C<sub>9</sub> fractions dominate, for both catalysts and at all temperatures. The C<sub>7</sub> fraction is unreacted toluene and the C<sub>9</sub> fraction is mainly, but not exclusively, ethyltoluene. The relative amount of the C<sub>9</sub> fraction, and also of ethyltoluene specifically, seems to reach a maximum at around 375 °C for both the catalysts. The fact that the yields of the C<sub>9</sub> and the C<sub>11</sub> fractions are lower at 400 °C than at 375 °C for both the catalysts indicates that catalytic cracking of monoethyl- and diethyltoluene becomes important at the higher temperature. The drop in yield when going from 375 °C to 400 °C is particularly pronounced for the mesopore-containing catalyst, which suggests that this material is a more active cracking catalyst. However, the yields are generally higher for the microporous/mesoporous catalyst than for the microporous catalyst, which is in line with the values for conversion of toluene. As can be seen from Table 2, several other fractions, in particular C<sub>8</sub>, C<sub>10</sub> and C<sub>11</sub>, are generated in non-negligible amounts.

The C<sub>11</sub> fraction can be attributed to dialkylation, *i.e.*, to formation of diethyltoluene and the ratio of monoalkylation to dialkylation has been calculated and is also given in Table 2. One may have anticipated that the larger pores of the mesopores-containing catalyst would have resulted in more dialkylation but that was evidently not the case. On the contrary, reaction over microporous/mesoporous HZSM-5 at the lowest temperature (325 °C) gives a very high ratio of mono- to dialkylation and reaction over microporous HZSM-5 at the same temperature gives the lowest ratio.

No attempts have been made to derive the formation mechanism for the C<sub>8</sub> and C<sub>10</sub> fractions. Several of the pathways shown in Scheme 1, as well as ethene oligomerization, may lead to such products. The fact that the difference in yield for the two catalysts is larger at 375 °C than at 325 °C indicates that pore clogging is a deactivation mechanism. It seems reasonable that the catalyst that contains mesopores is more resistant to clogging by high molecular weight carbonaceous materials than the catalyst with only micropores. The drop in reaction yield with both the catalysts when the temperature is raised to 400 °C is probably due to catalytic cracking of the reaction product becoming important, as was discussed above. Table 2 gives the relative amounts of the three regioisomers of ethyltoluene obtained with the two catalysts at the different temperatures. As can be seen, both the microporous/mesoporous and the microporous HZSM-5 give very little alkylation in *ortho* position. This is in agreement with previous studies on ethylation of toluene with ethene over HZSM-5 zeolite.<sup>16a</sup> Whereas the thermodynamic equilibrium for ethylation of toluene is *para* : *meta* : *ortho* 30–35 : 50 : 15–20 (values are temperature dependent), alkylation with ethene over HZSM-5 gives a much lower yield of the *ortho* isomer.<sup>16c</sup> Unmodified HZSM-5 has been reported to give a higher relative amount of the *meta* isomer and a somewhat lower relative amount of the *para* isomer. The regioselectivity also depends on the reaction temperature and on the acidity of the catalyst. A decrease in temperature results in an increase in the relative amount of the *para* isomer.<sup>7a</sup> The *para* selectivity also increases when the Brønsted acidity is reduced.<sup>16c</sup> By a proper choice of catalyst and reaction conditions a *para* selectivity well above 90% can be achieved. These deviations from the thermodynamical isomer ratio are caused by the fact that *ortho*-ethyltoluene has the largest and *para*-ethyltoluene the smallest minimum dimension. The product

ratio will depend on the relative rates of diffusion of the regioisomers. It has been demonstrated that the diffusion of the *para* isomer of ethyltoluene in the pores of a zeolite can be several orders of magnitude higher than that of the bulkier *ortho* and *meta* isomers.<sup>20</sup> The more slowly moving *ortho* and *meta* isomers remain within the zeolite and once the *para* isomer is generated as a result of the random isomerization that occurs under the influence of the acidic catalyst it rapidly diffuses out. The net result is that the relative amount of *para*-ethyltoluene can become very high and the relative amount of *ortho*-ethyltoluene, which is the most voluminous and therefore the most slowly diffusing isomer, virtually zero. Table 2 show that the *ortho* to *meta* to *para* ratio did not differ dramatically for the two types of catalysts. Thus, the large pores in the microporous/mesoporous material did not result in a higher relative yield of the more bulky *ortho* and *meta* isomers. For the catalyst with mesopores there was a substantial increase in the *meta* to *para* ratio with an increase in temperature. This is in agreement with previously reported trends.<sup>7a</sup> Reactions over the regular microporous catalyst gave almost the same *meta* to *para* ratio at the different temperatures, however. The effect of the ethene flow rate was investigated for microporous/mesoporous HZSM-5 at 375 °C. As can be seen in Table 2, neither the conversion of toluene, nor the product composition was much influenced by this parameter under the conditions studied.

## Conclusion

The microporous/mesoporous HZSM-5 catalyst gave a slightly higher conversion than the conventional microporous zeolite in the Friedel–Crafts alkylation of toluene with ethene. The yield of ethyltoluene was also somewhat higher with the former catalyst. For both catalysts the yield went through a maximum around 375 °C. The difference in yield obtained with the two catalysts increased with increasing temperature. This indicates that clogging of the pores with carbonaceous material is a deactivation mechanism at higher temperature. A catalyst that contains mesopores is likely to be more resistant to clogging than a catalyst that only contains micropores. Catalytic cracking of the products formed, *i.e.* ethyl- and diethyltoluene, is another possible reason for the decrease in yield at higher temperature. One might have expected the catalyst with mesopores to give a higher ratio of dialkylation to monoalkylation but this was not the case. On the contrary, the mesopore-containing catalyst gave a slightly higher selectivity for monoalkylation than the catalyst with only micropores. There was an interesting difference in regioselectivity for the two catalysts. Whereas the microporous zeolite gave a relatively constant *meta* to *para* ratio over the temperature interval studied, the *meta* to *para* ratio went from 48 : 52 at 325 °C to 59 : 32 at 400 °C for the microporous/mesoporous zeolite. Both catalysts gave very small yield of the *ortho* isomer.

## Acknowledgements

Cecilia Thorstensson at AkzoNobel Surface Chemistry is acknowledged for help with the GC-MS analysis. The Swedish Research Council is acknowledged for financial support.

## Notes and references

- 1 S. Kulprathipanja, *Microporous Zeolites in Industrial Catalysis and Separation*, Wiley-VCH Verlag GmbH, Weinheim, 2010.
- 2 (a) M. Guidotti, C. Canaff, J. M. Coustard, P. Magnoux and M. Guisnet, *J. Catal.*, 2005, **230**, 375; (b) E. G. Derouane, C. J. Dillon, D. Bethell and S. B. Derouane-Abd Hamid, *J. Catal.*, 1999, **187**, 209; (c) M. E. Davis, *Nature*, 2002, **417**, 813.
- 3 (a) R. Srivastava, M. Choi and R. Ryoo, *Chem. Commun.*, 2006, 4489; (b) A. Taguchi and F. Schüth, *Microporous Mesoporous Mater.*, 2005, **77**, 1; (c) Z. Bohström, I. Rico-Lattes and K. Holmberg, *Green Chem.*, 2010, **12**, 1861; (d) Z. Bohström, *J. Porous Mater.*, 2012, **19**, 921; (e) Z. Bohström and K. Holmberg, *J. Mol. Catal. A: Chem.*, 2013, **366**, 64.
- 4 Y. Han, N. Li, L. Zhao, D. Li, X. Xu, S. Wu, Y. Di, C. Li, Y. Zou, Y. Yu and F.-S. Xiao, *J. Phys. Chem. B*, 2003, **197**, 7551.
- 5 F.-S. Xiao, L. Wang, C. Yin, K. Lin, Y. Di, J. Li, R. Xu, D. Su, R. Schlögl, T. Yokoi and T. Tatsumi, *Angew. Chem., Int. Ed.*, 2006, **45**, 3090.
- 6 (a) Z. Yang, Y. Xia and R. Mokaya, *Adv. Mater.*, 2004, **16**, 727; (b) H. C. Li, Y. Sakamoto, Z. Liu, T. Ohsuna, O. Terasaki, M. Thommes and S. Che, *Microporous Mesoporous Mater.*, 2007, **106**, 174; (c) Y. M. Fang and H. Q. Hu, *J. Am. Chem. Soc.*, 2006, **128**, 10636; (d) W.-C. Li, A.-H. Lu, R. Palkovits, W. Schmidt, B. Spliethoff and F. Schüth, *J. Am. Chem. Soc.*, 2005, **127**, 12595; (e) R. Srivastava, N. Iwasa, S.-I. Fujita and M. Arai, *Chem.–Eur. J.*, 2008, **14**, 9507; (f) H. Wang and T. J. Pinnavaia, *Angew. Chem., Int. Ed.*, 2006, **45**, 7603; (g) M. Choi, H. S. Cho, R. Srivastava, C. Venkatesan, D. Choi and R. Ryoo, *Nat. Mater.*, 2006, **5**, 718; (h) K. Egeblad, M. Kustova, S. K. Klitgaard, K. Zhu and C. H. Christensen, *Microporous Mesoporous Mater.*, 2007, **101**, 214.
- 7 (a) J. Cejka, B. Wichterlov and S. Bednarova, *Appl. Catal., A*, 1991, **79**, 215; (b) S. Rummel, S. M. Yunusov, H. Langguth and V. B. Shuth, *Russ. Chem. Bull.*, 1999, **48**, 2083.
- 8 L. Wang, Z. Zhang, C. Yin, Z. Shan and F.-S. Xiao, *Microporous Mesoporous Mater.*, 2010, **131**, 58.
- 9 P. Punyapalikul, S. Soonglerdsongpha, C. Kanlayaprasit, C. Ngamcharussrivichai and S. Khaodhiar, *J. Hazard. Mater.*, 2009, **171**, 491.
- 10 S. Brunauer, P. H. Emmett and E. Teller, *J. Am. Chem. Soc.*, 1938, **60**, 309.
- 11 E. P. Barrett, L. G. Joyner and P. P. Halenda, *J. Am. Chem. Soc.*, 1951, **73**, 373.
- 12 (a) A. Hinz, M. Skoglundh, E. Fridell and A. Andersson, *J. Catal.*, 2001, **201**, 247; (b) H. H. Ingelsten, Å. Hildesson, E. Fridell and M. Skoglundh, *J. Mol. Catal. A: Chem.*, 2004, **209**, 199.
- 13 S. Z. Chen, K. Huddersman, D. Keir and L. V. C. Rees, *Zeolites*, 1988, **8**, 106.
- 14 K. S. W. Sing, D. H. Everett, R. A. W. Haul, L. Moscou, R. A. Pierotti, J. Rouquerol and T. Siemieniowska, *Pure Appl. Chem.*, 1985, **57**, 603.
- 15 (a) Z.-M. Wang, M. Yamaguchi, I. Goto and M. Kumagai, *Phys. Chem. Chem. Phys.*, 2002, **2**, 3007; (b) A. A. Tsyganenko, D. V. Pozdnyakov and V. N. Filimonov,

- J. Mol. Struct.*, 1975, **29**, 299; (c) A. A. Tsyganenko and V. N. Filimonov, *J. Mol. Struct.*, 1973, **19**, 579; (d) A. A. Tsyganenko and P. P. Mardilovich, *J. Chem. Soc., Faraday Trans.*, 1996, **92**, 4843.
- 16 (a) B. S. Kwak and T. J. Kim, *Appl. Catal., A*, 1999, **188**, 99; (b) L. Z. Chen and Y. Q. Feng, *Zeolites*, 1992, **11**, 347; (c) F. Lónyi, J. Engelhardt and D. Kalló, *Zeolites*, 1991, **11**, 169; (d) S. Sealy and Y. Traa, *Appl. Catal., A*, 2005, **294**, 273; (e) W. W. Kaeding, L. B. Young and C.-C. Chu, *J. Catal.*, 1984, **89**, 267; (f) V. Mavrodinova, Ch. Minchev, V. Penchev and H. Lechert, *Zeolites*, 1985, **4**, 217.
- 17 (a) N. Rahimi and R. Karimzadeh, *Appl. Catal., A*, 2011, **398**, 1; (b) T.-C. Tsai, S.-B. Liu and I. Wang, *Appl. Catal., A*, 1999, **181**, 355.
- 18 C. Song, J. Garces and Y. Sugi, Shape Selective Catalysis - Chemical Synthesis and Hydrocarbon Processing, *ACS Symposium Series*, Washington DC, 1999.
- 19 (a) A. Marcilla, A. Gómez-Siurana and F. J. Valdés, *Microporous Mesoporous Mater.*, 2008, **109**, 420; (b) M. J. B. Souza, F. A. N. Fernandes, A. M. G. Pedrosa and A. S. Araujo, *Fuel Process. Technol.*, 2008, **89**, 819.
- 20 N. Y. Chen, W. W. Kaeding and F. G. Dwyer, *J. Am. Chem. Soc.*, 1979, **101**, 6783.